Prepared for submission to JHEP

Axial resonances $a_1(1260)$, $b_1(1235)$ and their decays from the lattice

C. B. Lang,[a] **Luka Leskovec,**[b] **Daniel Mohler,**[c] **and Sasa Prelovsek**[b,d]

[a] *Institute of Physics, University of Graz, A–8010 Graz, Austria*
[b] *Jozef Stefan Institute, 1000 Ljubljana, Slovenia*
[c] *Fermi National Accelerator Laboratory, Batavia, Illinois 60510-5011, USA*
[d] *Department of Physics, University of Ljubljana, 1000 Ljubljana, Slovenia*

E-mail: christian.lang@uni-graz.at, luka.leskovec@ijs.si, dmohler@fnal.gov, sasa.prelovsek@ijs.si

Abstract: The light axial-vector resonances $a_1(1260)$ and $b_1(1235)$ are explored in $N_f=2$ lattice QCD by simulating the corresponding scattering channels $\rho\pi$ and $\omega\pi$. Interpolating fields $\overline{q}q$ and $\rho\pi$ or $\omega\pi$ are used to extract the s-wave phase shifts for the first time. The ρ and ω are treated as stable and we argue that this is justified in the considered energy range and for our parameters $m_\pi \simeq 266$ MeV and $L \simeq 2$ fm. We neglect other channels that would be open when using physical masses in continuum. Assuming a resonance interpretation a Breit-Wigner fit to the phase shift gives the $a_1(1260)$ resonance mass $m_{a_1}^{\rm res} = 1.435(53)(^{+0}_{-109})$ GeV compared to $m_{a_1}^{\rm exp} = 1.230(40)$ GeV. The a_1 width $\Gamma_{a_1}(s) \equiv g^2 p/s$ is parametrized in terms of the coupling and we obtain $g_{a_1\rho\pi} = 1.71(39)$ GeV compared to $g_{a_1\rho\pi}^{\rm exp} = 1.35(30)$ GeV derived from $\Gamma_{a_1}^{\rm exp} = 425(175)$ MeV. In the b_1 channel, we find energy levels related to $\pi(0)\omega(0)$ and $b_1(1235)$, and the lowest level is found at $E_1 \gtrsim m_\omega + m_\pi$ but is within uncertainty also compatible with an attractive interaction. Assuming the coupling $g_{b_1\omega\pi}$ extracted from the experimental width we estimate $m_{b_1}^{res} = 1.414(36)\big(^{+0}_{-83}\big)$.

Keywords: decay width, axial mesons, scattering, lattice QCD

arXiv:1401.2088v2 [hep-lat] 5 May 2014

Contents

1 Introduction **1**

2 Lattice setup **3**

3 Discussion of assumptions **3**

4 Masses of π, ρ, ω **5**

5 Energies in a_1 and b_1 channels **6**

6 Resonance parameters for $a_1(1260)$ **8**

7 Analysis of the b_1 channel **10**

8 Conclusions and outlook **11**

A Wick contractions and the correlation matrix **11**

A.1 The $\rho\pi$ s-wave correlation matrix 11

A.2 The $\omega\pi$ s-wave correlation matrix 12

1 Introduction

Ab-initio lattice simulations of light mesons are complicated by the fact that the majority of these states are hadronic resonances and therefore decay under the strong interaction. This is the case also for all vector ($J^P = 1^-$) and axial-vector ($J^P = 1^+$) mesons. The vector resonance ρ is the only hadronic resonance that has been treated on the lattice by several collaborations [1–6], taking into account its unstable nature and extracting its resonance mass as well as the width. First steps in this direction were also made recently for the vector resonance $K^*(892)$ [7], where mass and width were extracted.

In the present paper we aim at simulating the ground state axial-vector resonances $a_1(1260)$ and $b_1(1235)$ with $I^G(J^{PC}) = 1^-(1^{++})$ and $1^+(1^{+-})$, respectively, taking into account their strong decays $a_1 \to \rho\pi$ and $b_1 \to \omega\pi$. The experimental mass and width $\Gamma_{b_1} = 142 \pm 9$ MeV of the $b_1(1235)$ are known rather precisely. The determination of the width for the broader a_1 from the lattice is important in view of its large uncertainty $\Gamma_{a_1} = 250 - 600$ MeV assigned by the Particle Data Group [8]. While most experiments and phenomenological extractions agree on the mass of the a_1 leading to a PDG value of $m_{a_1}^{\mathrm{PDG}} = 1.230(40)$ GeV [8], determinations of Γ_{a_1} from diffractive processes where the extraction of the resonance parameters has considerable model dependence [9], deviate substantially from an analysis of data obtained from $\tau \to a_1\nu$ [10]. As an example for data

obtained from a diffractive process, a recent COMPASS measurement published in 2010 [11] provides a much smaller error-bar $\Gamma_{a_1} = 367 \pm 9^{+28}_{-25}$ MeV.

Our simulation is the first attempt at extracting the s-wave scattering phase shifts for $\rho\pi$ or $\omega\pi$ channels in lattice QCD. We are interested in the energy region covering the lowest resonance states, i.e., up to $\mathcal{O}(1.5)$ GeV. To determine the phase shift in the a_1 channel, for example, we first extract the discrete energy levels of the system with $I^G(J^{PC}) = 1^-(1^{++})$ and total momentum zero. These levels are related to the resonant state a_1 as well as the two-particle states $\rho(\mathbf{p})\pi(-\mathbf{p})$ with $\mathbf{p} \simeq \frac{2\pi}{L}\mathbf{n}$. Both, $\overline{q}q$ as well as meson-meson interpolators are implemented. The energy levels render the scattering phase shifts via Lüscher's relation [12–15] and the energy-dependence of the phase shift allows the determination of the resonance mass as well as the width.

Within this simulation we assume the ρ and ω to be stable. Furthermore, additional decay channels of the a_1 and b_1 are neglected. Our assumptions and their justification are addressed in section 3.

The decay $b_1 \to \omega\pi$ was simulated on the lattice earlier only by McNeile and Michael [16], where the Wick contractions with back-tracking loops (i.e., quark lines running from source to source or from sink to sink) were omitted. The width $\Gamma[b_1 \to \omega\pi]$ was extracted based on the amplitude method [17] and reasonable agreement with experiment was found (see figure 3 of [16]). The a_1 has never been simulated taking into account its strong decay, with exception of our preliminary results [18].

While in quantum field theory with dynamical quarks one expects to find contributions of the intermediate meson-meson states even in correlators of $\overline{q}q$, in practice such signals were not clearly observed. The masses of a_1 and b_1 were previously determined by a number of lattice collaborations within the so-called single-hadron approach. In this approach only $\bar{q}q$ interpolators are used. One assumes that the coupling to two-particle interpolators of the type $V\pi$ ($V = \rho, \omega$) is negligible and that the mass equals the observed ground state energy level $m = E$ (for $P = 0$). It turned out to be a better strategy to include meson-meson interpolators explicitly in the set of source and sink operators and to study the meson-meson system this way. Indeed in this more complete, coupled system level shifts as compared to the non-interaction case can be observed. The assumption that two-particle interpolators may be neglected is particularly questionable in our situation, since $V(0)\pi(0)$ with $E \simeq m_V + m_\pi < m_{a_1,b_1}$ is the ground state of the system.

The a_1 and b_1 mesons have been extensively studied also by non-lattice methods. Weinberg derived $m_{a_1}/m_\rho \simeq \sqrt{2}$ based on spectral functions of currents [19]. More recently, axial mesons emerged as dynamically generated resonances in the study of scattering between pseudoscalar and vector mesons based on chiral Lagrangians [20–22]. Unitarized Chiral Perturbation Theory models render poles related to axial mesons dynamically although these are not present in the original Lagrangian [23]. This approach was used also to determine the dependence of their masses and widths as a function of number of colors (N_c). It was found that this dependence significantly deviates from the expectation $M \propto N_c^0$ and $\Gamma \propto 1/N_c$ for pure $\overline{q}q$ structure [24]. The chiral properties and issues related to chiral restoration were considered for example in [25, 26].

After introducing our lattice setup, we address the assumptions made within this study.

$N_L^3 \times N_T$	β	a[fm]	L[fm]	#cfgs	m_π[MeV]
$16^3 \times 32$	7.1	0.1239(13)	1.98	280	266(4)

Table 1. Parameters of the $N_f = 2$ gauge configurations [3].

Afterwards we present the masses of the scattering particles π, ρ and ω in section 4. The interpolators and the energy spectra in the a_1 and b_1 channels are discussed in section 5, while the Wick contractions are relegated to the appendix. The analysis related to the scattering phase shifts and the resonance parameters is given in two subsequent sections followed by our conclusions.

2 Lattice setup

The simulation is based on one ensemble of $N_f = 2$ gauge configurations with clover Wilson u/d quarks, generated by the authors of [27, 28]. The dynamical and valence u/d quarks have the same mass corresponding to $m_\pi = 266(4)$ MeV. The parameters of the ensemble are shown in table 1, while more details are given in [3]. Due to the limited data for just a single ensemble, our determination of the lattice spacing a reported in [3] results from taking a typical value of the Sommer parameter r_0. The uncertainty associated with this choice might lead to a small shift of all dimensionful quantities.

The sea and valence quarks obey periodic boundary conditions in space. Valence quark propagators periodic and anti-periodic in time are combined into so-called "$P + A$" propagators, which effectively extends the time direction to $2N_T = 64$ [3]. We use translation invariance in t to sum over correlators from sources in every time slice. Errors on all values provided are obtained from single-elimination jack-knife procedure. For each jack-knife subset the full analysis of eigenstates and the subsequent evaluations are done giving the statistical variance of the results.

The rather small volume $V = 16^3 \times 32$ ($L \simeq 2$ fm) simplifies the use of the powerful full distillation method [29], which allows for the computation of all contractions for the correlation matrix with $\overline{q}q$ and $V\pi$ interpolators. A small box also has the advantage that the effect of $\rho \to 2\pi$ and $\omega \to 3\pi$ is less significant in our simulation with total momentum zero.

3 Discussion of assumptions

In this section we discuss the assumptions in our study of two channels at hand. We assume that for $E < 1.5$ GeV the a_1 and b_1 channels are dominated by $\rho\pi$ and $\omega\pi$ scattering in s-wave, and that ρ and ω are stable. Therefore we assume that the effects of other channels, higher partial waves and ρ/ω decays do not significantly affect our conclusions.

Let us first focus on the effect of $\rho \to 2\pi$ decay in $\rho\pi$ scattering. In the absence of a rigorous framework for the analysis of $a_1 \to 3\pi$ we omit 3π lattice interpolators. We expect that they have little effect on the energy levels in the relevant energy region. In order to address this, we first have to emphasize the role of our lattice environment, in particular

the unphysical high pion mass and the effect of the lattice volume. The analysis relies on the discrete energy eigenstates of the correlators between a set of lattice operators. The relevance of an interpolator O_i for an eigenstate n can be estimated from its overlap $\langle O_i|n\rangle$. Allowing for additional $\pi\pi\pi$ interpolators in 1^{++} channel in principle allows for $\rho \to \pi\pi$ transition in $\rho\pi$ scattering. This might lead to shifts of 1^{++} energy levels (compared to the uncoupled $\rho - \pi\pi$ situation) if $\pi\pi$ and ρ levels are close in energy, i.e., within $\simeq \Gamma_\rho$. We know from earlier work [3] that for our lattice parameters the ground state at rest $\rho(0)$ has negligible overlap with the $\pi(1)\pi(-1)$ operator [1]. This is because this lowest two-pion interpolator allowed by the conservation of momentum and angular momentum has energy $2(m_\pi^2 + (2\pi/L)^2)^{1/2} \simeq 1.4$ GeV $\gg m_\rho$ [3]. The $\rho(1)$ with momentum $p = 2\pi/L$ would have been more significantly affected by the $\pi(1)\pi(0)$ decay channel due to its vicinity. In this study we restrict ourselves to $E < 1.5$ GeV and $\rho(p)$ has momentum $p < 2\pi/L$ for both energy levels of interest in Table 3. Although the $\rho \to \pi\pi$ channel is formally open as soon as $\sqrt{s_{\pi\pi}} > m_\rho$, we expect that the $\rho\pi \to 3\pi$ decay channel does not significantly influence the two lowest energy levels in our energy region

$$E < E_{\rho(1)\pi(-1)} \simeq (m_\rho^2 + (\tfrac{2\pi}{L})^2)^{1/2} + (m_\pi^2 + (\tfrac{2\pi}{L})^2)^{1/2} \simeq 1.7 \text{ GeV} . \tag{3.1}$$

In order to avoid $\rho(1) \to \pi(1)\pi(0)$ we restricted our simulation to the total momentum $P \equiv |\mathbf{P}| = 0$, where the possible effect of vector meson decay is least significant.

Let us point out that analytical frameworks for rigorous multi-channel treatment on the lattice have been proposed, but their realization in practice remains a serious challenge. Analytic approaches for the scattering of unstable particles (with some emphasis on s-wave scattering) in the finite volume were recently formulated in [30], while the related challenging problem of three particles in a finite box was analytically considered in [31–34]. In Ref. [30] the approach was applied to study the effect of the $\rho \to \pi\pi$ decay to the $\rho\pi$ scattering. Its effect on the discrete spectrum at zero momentum is found to be negligible on our lattice with $L \simeq 2$ fm and $m_\pi \simeq 266$ MeV in the region of interest $E < E_{\rho(1)\pi(-1)} \simeq 1.7$ GeV where a_1 resides [30]. The effect of $\omega \to 3\pi$ decay for $\omega\pi$ scattering has not been studied in detail, but its influence is suppressed due to the narrow width $\Gamma_\omega^{exp} \simeq 8$ MeV and since at least two pions must have non-vanishing momentum when ω decays at rest.

More generally, lattice interpolators with intrinsically higher energy have very little overlap with lower energy eigenstates and therefore little impact on these eigen-energies. So the threshold (the sum of masses) to some channels may be formally open but the actual eigenstate energy may be considerably higher. In that spirit we argue that interpolators which represent such higher energy content may be neglected when studying only low energy eigenstates.

In addition to $\rho\pi$ and $\omega\pi$ there are further two-meson decay channels to consider. The a_1 can also couple to $f_0(500)\pi$ and $f_0(980)\pi$ in p-wave, which goes to three pions. The lowest possible interpolator with three pions combining to total spin 1 needs pions with non-vanishing momentum units like $\pi(0)\pi(1)\pi(-1)$ and thus – for our parameters – has an energy clearly above the range considered here.

[1] The meson momenta given in parenthesis $M(\mathbf{p})$ are in physical units or in units of $2\pi/L$.

$m_\pi a$	$m_\rho a$	$m_\omega a$
0.1673(16)	0.5107(40)	0.514(15)

Table 2. The masses of scattering particles in lattice units with $a^{-1} \simeq 1.59$ GeV.

Another possible coupled channel for a_1 and b_1 is $K\bar{K}^*$ in s-wave; its threshold would be close to 1.4 GeV, but it cannot be produced from $\bar{u}d$, $\pi\rho$ or $\pi\omega$ interpolators in our simulation with only $N_f = 2$ dynamical quarks. The $K\bar{K}^*$ could appear only by explicitly incorporating the corresponding interpolator with s quarks as valence quarks, but $K\bar{K}^* \to \bar{u}d$ transition would be Zweig suppressed and we omit such interpolators.

The b_1 channel also couples to $\eta_2\rho$, its contribution might be relevant only above threshold for energies above $\mathcal{O}(1.5)$ GeV and we omit this interpolator.[2] To summarize, we assume that the elastic scattering $\rho\pi$ and $\omega\pi$ dominates both channels in the energy region of interest and rely on the same assumption when extracting $\Gamma_{a_1\to\rho\pi}$ and $\Gamma_{b_1\to\omega\pi}$ from the experimental data. We note that the inelastic scattering with coupled channels has not been treated in lattice simulations yet, while the analytic frameworks for this challenging problem were developed, for example, in [34–37].

4 Masses of π, ρ, ω

The masses of the scattering particles π, ρ, ω are needed for the position of the thresholds and we collect them in table 2. We use m_π as determined in [3].

The ρ mass in table 2 was extracted as $m_\rho = E_\rho(p = 0)$ in [3] and is indeed found close to m_ρ^{res} in all simulations [1–6]. The ω energy is calculated using quark-antiquark interpolators $\mathcal{O}^{s=n}_{1-5}$ given by Eq. (21) of [3] with five different Dirac/space structures, while flavor is replaced with $\bar{u}u + \bar{d}d$. This approach is consistent with our approximation of treating $\rho(p)$ and $\omega(p)$ with $p \ll 2\pi/L$ as stable; this holds well for the narrow ω and is commonly applied also for the broader ρ. The distillation method enables straightforward calculation of the disconnected contributions to ω and the final correlators are averaged over all initial time-slices and three polarizations. The disconnected contribution is small and we find $m_\omega \simeq m_\rho$ as expected. The value of m_ω follows from a 2-exponent fit in range $t = 3 - 12$ using interpolators $\mathcal{O}^n_{1,2,3,5}$ and $t_0 = 2$. This is a conservative choice with a comparatively large uncertainty and is fully consistent with the result of other possible choices.

[2] The η_2 corresponds to η for $N_f = 2$ dynamical quarks and has a mass between the η and the η'

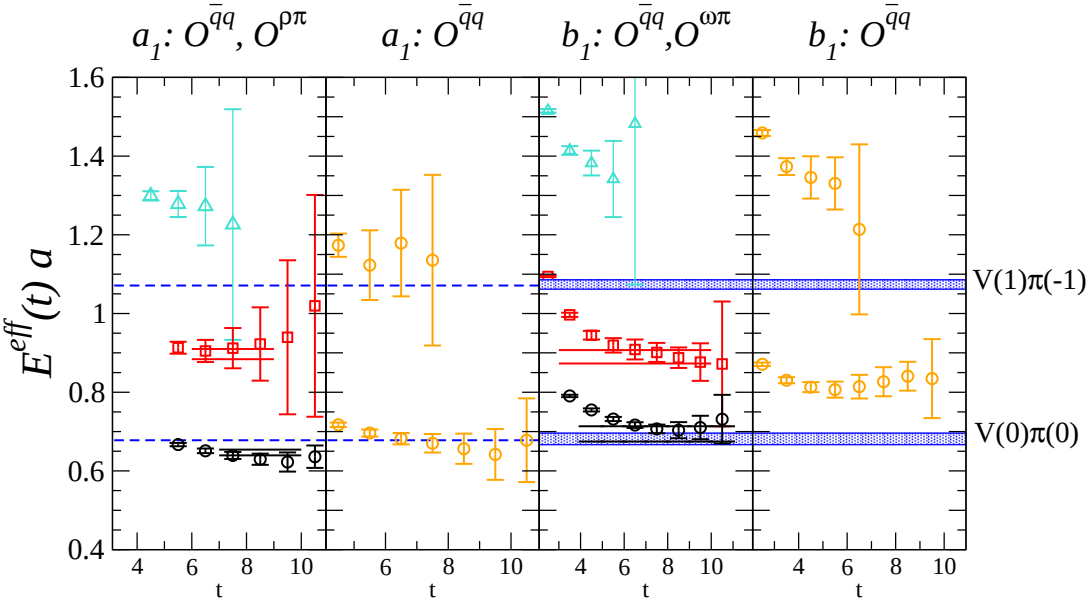

Figure 1. Effective energies $E_n^{\rm eff}a$ in the a_1 and b_1 channels, that correspond to the energy levels $E_n a$ in the plateau region. The horizontal lines indicate the $m_V + m_\pi$ threshold and the energy of a non-interacting $V(1)\pi(-1)$ state, where $V = \rho$ for a_1 and $V = \omega$ for b_1. We compare the results when $\mathcal{O}^{V\pi}$ is included in or excluded from the interpolator basis.

5 Energies in a_1 and b_1 channels

The interpolators for the a_1 channel with $J^{PC} = 1^{++}$, $|a_1^-\rangle = -|I = 1, I_3 = -1\rangle$, $P{=}0$ and polarization i are

$$
\begin{aligned}
\mathcal{O}_1^{\bar{q}q} &= \sum_{\mathbf{x}} \bar{u}(x)\ \gamma_i\ \gamma_5\ d(x)\ , \qquad (5.1)\\
\mathcal{O}_2^{\bar{q}q} &= \sum_{\mathbf{x},j} \bar{u}(x)\overleftarrow{\nabla}_j\ \gamma_i\ \gamma_5\ \overrightarrow{\nabla}_j\ d(x)\ ,\\
\mathcal{O}_3^{\bar{q}q} &= \sum_{\mathbf{x},j,l} \epsilon_{ijl}\ \bar{u}(x)\ \gamma_j\ \tfrac{1}{2}[\overrightarrow{\nabla}_l - \overleftarrow{\nabla}_l]\ d(x)\ ,\\
\mathcal{O}^{\rho\pi} &= \frac{1}{\sqrt{2}}[\pi^0(\mathbf{0})\rho^-(\mathbf{0}) - \rho^0(\mathbf{0})\pi^-(\mathbf{0})]\\
&= \frac{1}{2}\Bigg(\sum_{\mathbf{x_1}}[\bar{u}(x_1)\gamma_5 u(x_1) - \bar{d}(x_1)\gamma_5 d(x_1)]\sum_{\mathbf{x_2}}\bar{u}(x_2)\gamma_i d(x_2)\\
&\qquad - \sum_{\mathbf{x_1}}[\bar{u}(x_1)\gamma_i u(x_1) - \bar{d}(x_1)\gamma_i d(x_1)]\sum_{\mathbf{x_2}}\bar{u}(x_2)\gamma_5 d(x_2)\Bigg)\ ,
\end{aligned}
$$

where $x_i = (\mathbf{x}_i, t)$ and ∇ denotes the covariant derivative. The ρ and π mesons are separately projected to zero momentum in $\mathcal{O}^{\rho\pi}$. We do not implement the interpolator $\rho(1)\pi(-1)$ (the argument ±1 indicates momenta $\pm 2\pi/L$) since we concentrate on the lower energy region $E < E_{\rho(1)\pi(-1)} \simeq 1.7$ GeV.

n	t_0	interp.	fit range	$\frac{\chi^2}{\text{d.o.f}}$	Ea	$\frac{E=\sqrt{s}}{[\text{GeV}]}$	pa	δ [°]	$\frac{p\cot(\delta)}{\sqrt{s}}$
1	5	$\mathcal{O}^{\bar{q}q}_{1,2}, \mathcal{O}^{\rho\pi}$	7-10	1.1	0.6468(73)	1.030(12)	i 0.0861(95)	i 23(14)	0.34(14)
2	5	$\mathcal{O}^{\bar{q}q}_{1,2}, \mathcal{O}^{\rho\pi}$	6-9	0.015	0.8977(133)	1.430(21)	0.272(10)	88.9(5.9)	0.005(31)

Table 3. Energies and phases in the a_1 channel with $I^G(J^{PC}) = 1^-(1^{++})$ and $P = 0$, where $a^{-1} \simeq 1.59$ GeV. Both levels were obtained using a 1 exponential fit. The p give the eigen-momenta of the interacting system determined from the energy levels according to Eq. (6.1). The ground state is below $\rho\pi$ threshold, so p and δ are imaginary, while $p\cot\delta$ is real.

n	t_0	interp.	fit range	$\frac{\chi^2}{\text{d.o.f}}$	Ea	$\frac{E=\sqrt{s}}{[\text{GeV}]}$	pa	δ [°]	$\frac{p\cot(\delta)}{\sqrt{s}}$
1	3	$\mathcal{O}^{\bar{q}q}_{1,2,4}, \mathcal{O}^{\omega\pi}$	4-11	0.12	0.694(19)	1.105(31)	0.057(45)	−3.0(6.3)	−1.6(2.2)
2	2	$\mathcal{O}^{\bar{q}q}_{1,3}, \mathcal{O}^{\omega\pi}$	3-10	0.049	0.890(17)	1.418(27)	0.264(13)	93.5(7.5)	−0.018(38)

Table 4. Similar as table 3 but for b_1 channel with $I^G(J^{PC}) = 1^+(1^{+-})$. Both levels were obtained using a 2 exponential fit. The second level is consistent with threshold energy $m_\pi + m_\omega$ due to relatively large uncertainties of E_2 and m_ω, and the corresponding phase is consistent with $\delta \simeq 0$. The uncertainty in m_ω has negligible effect on δ for the second level.

Similarly, for the b_1 channel with $J^{PC} = 1^{+-}$ and $|b_1^-\rangle = -|I = 1, I_3 = -1\rangle$ we use

$$\begin{aligned}
\mathcal{O}^{\bar{q}q}_1 &= \sum_{\mathbf{x}} \bar{u}(x)\ \gamma_i\ \gamma_t\ \gamma_5\ d(x)\ , \\
\mathcal{O}^{\bar{q}q}_2 &= \sum_{\mathbf{x},j} \bar{u}(x) \overleftarrow{\nabla}_j\ \gamma_i\ \gamma_t\ \gamma_5\ \overrightarrow{\nabla}_j\ d(x)\ , \\
\mathcal{O}^{\bar{q}q}_3 &= \sum_{\mathbf{x}} \bar{u}(x)\ \gamma_5\ \tfrac{1}{2}[\overrightarrow{\nabla}_i - \overleftarrow{\nabla}_i]\ d(x)\ , \\
\mathcal{O}^{\bar{q}q}_4 &= \sum_{\mathbf{x}} \bar{u}(x)\ \gamma_t\ \gamma_5\ \tfrac{1}{2}[\overrightarrow{\nabla}_i - \overleftarrow{\nabla}_i]\ d(x)\ , \\
\mathcal{O}^{\omega\pi} &= \omega(\mathbf{0})\pi^-(\mathbf{0}) = \frac{1}{\sqrt{2}} \sum_{\mathbf{x_1}} [\bar{u}(x_1)\gamma_i u(x_1) + \bar{d}(x_1)\gamma_i d(x_1)] \sum_{\mathbf{x_2}} \bar{u}(x_2)\gamma_5 d(x_2)\ ,
\end{aligned} \tag{5.2}$$

where, again, ω and π are separately projected to zero momentum.

All quark fields q in Eqs. (5.1), (5.2) are smeared according to the distillation method [29], thus effectively replaced by $\sum_{k=1}^{N_v} v^{(k)} v^{(k)\dagger} q$ with $N_v = 96$, where the $v^{(k)}$ denote the Laplacian eigenvectors of the time slice.

The energy spectrum E_n is extracted from the correlation matrix

$$C_{jl}(t) = \frac{1}{N_T} \sum_{t_i} \langle \mathcal{O}_j^\dagger(t_i + t) | \mathcal{O}_l(t_i) \rangle = \sum_n Z_{jn} Z^*_{ln} e^{-E_n t} \tag{5.3}$$

averaged over all initial times t_i. The Wick contractions for both channels are presented in figures 3 and 4 of the appendix. In particular in the b_1 channel a rather large number of diagrams appears. Expressions for various elements of the correlation matrix in terms of those Wick contractions are also provided in the appendix. We evaluate all the Wick contractions using the distillation method, which handles efficiently also those with back-tracking quark lines.

The variational method with the generalized eigenvalue equation

$$C(t)\, v_n(t) = \lambda_n(t)\, C(t_0)\, v_n(t) \tag{5.4}$$

is applied to extract the discrete spectrum E_n [12, 38–40]. The resulting eigenvalues $\lambda_n(t) \sim \mathrm{e}^{-E_n(t-t_0)}$ give the effective energies $E_n^{\mathrm{eff}}(t) \equiv \log[\lambda_n(t)/\lambda_n(t+1)] \to E_n$. The spectrum E_n is extracted using correlated fits to $\lambda_n(t)$.

The resulting spectrum E_n is shown in figure 1, where effective energies are plotted for the cases when $\mathcal{O}^{V\pi}$ is included or excluded from the correlation matrix. The horizontal lines indicate the position of the threshold $m_V + m_\pi$ (which has sizable uncertainty in the b_1 channel), and the energy of the non-interacting $V(1)\pi(-1)$ system.

We concentrate on the spectrum obtained including $\mathcal{O}^{V\pi}$, which is shown in the first and third pane of figure 1 and listed in tables 3 and 4. The lowest levels (circles) are near the $m_V + m_\pi$ threshold, as expected, and its dominant component is the $V(0)\pi(0)$ two-particle interpolator. The second level (squares) arises due to the presence of $a_1(1260)$ or $b_1(1235)$ resonances in these channels. The next level would be expected close to $V(1)\pi(-1)$, but we do not expect to see it since the corresponding interpolator is not implemented in Eqs. (5.1) and (5.2).

The third levels in figure 1 in both channels are noisy and unreliable, so we refrain from presenting quantitative results. Both levels correspond to masses close to 2 GeV or above, so we see no indication for the possible existence of $a_1(1420)$, which was introduced to explain recent preliminary data by COMPASS in $a_1 \to f_0\pi$ channel [41]. The third level in b_1 channel might be related to the observed $b_1(1960)$.

6 Resonance parameters for $a_1(1260)$

The position of the 1^{++} ground state below $m_\rho + m_\pi$ threshold indicates that the energy of ρ and π is smaller if they are in the box together than if they are in the box alone. The negative energy shift is consistent with an attractive interaction in the resonant a_1 channel. We proceed to extract the $\rho\pi$ phase shifts and the resonance parameters of $a_1(1260)$. Outside the interaction region the mesons are considered as free particles and the energy levels E are related to the momenta p of the two-particle state $\rho(p)\pi(-p)$ through

$$E = \sqrt{m_\pi^2 + p^2} + \sqrt{m_\rho^2 + p^2}\ , \tag{6.1}$$

where we employ the continuum dispersion relation which applies well for the small momenta $p < 2\pi/L$ of interest [3]. The s-wave phase shifts δ for $\rho\pi$ scattering at these values of p are given by the well known Lüscher relation [15]

$$\tan\delta(p) = \frac{\sqrt{\pi}\ p\ L}{2\ \mathcal{Z}_{00}\left(1; (\frac{pL}{2\pi})^2\right)}\ , \tag{6.2}$$

which applies above and below threshold for elastic scattering. The d-wave to s-wave amplitude ratio for $a_1 \to \rho\pi$ is -0.062 ± 0.02 experimentally [8], therefore we safely neglect the d-wave in Eq. (6.2). The relation (6.2) also neglects the contribution of the $f_0\pi$

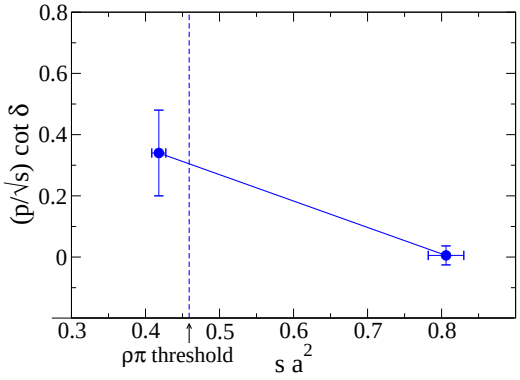

Figure 2. We show $\frac{p}{\sqrt{s}} \cot\delta(s)$ with linear interpolation according to Eq. (6.4). At threshold the value is $[(m_\rho + m_\pi)a_{l=0}^{\rho\pi}]^{-1}$, while the position of the zero gives the resonance mass.

resonance	$a_1(1260)$			$b_1(1235)$	
quantity	$m_{a_1}^{\text{res}}$ [GeV]	$g_{a_1\rho\pi}$ [GeV]	$a_{l=0}^{\rho\pi}$ [fm]	$m_{b_1}^{\text{res}}$ [GeV]	$g_{b_1\omega\pi}$ [GeV]
lat	$1.435(53)(^{+0}_{-109})$	1.71(39)	0.62(28)	$1.414(36)(^{+0}_{-83})$	input
exp	1.230(40)	1.35(30)	-	1.2295(32)	0.787(25)

Table 5. The resulting Breit-Wigner masses m^{res} together with the couplings g for $a_1 \to \rho\pi$ and $b_1 \to \omega\pi$, which are related to the Breit-Wigner width $\Gamma \equiv g^2 p/s$. For the resonance masses the second uncertainty given stems from the systematic uncertainty in extracting the first excited state reliably. This uncertainty has negligible effect on the extracted coupling. The experimental values for the couplings g are derived from the measured total widths [8] since the branching ratios to $V\pi$ have not been measured, but are expected to be largely dominant. The lattice value for the resonance mass of $b_1(1235)$ is obtained assuming experimental $g_{b_1\omega\pi}^{\text{exp}}$. All results are for our value of $m_\pi \simeq 266$ GeV.

channel, which is known to be subdominant experimentally; this simplifies one equation with several unknowns to the equation (6.2) with one unknown δ for $\rho\pi$ scattering. The $K\bar{K}^*$ intermediate state can not appear in our $N_f = 2$ simulation with chosen interpolators, therefore the corresponding scattering parameters do not feature in the Lüscher's relation.

The ground state below the $m_\rho + m_\pi$ threshold renders imaginary p and real $p\cot\delta$ in table 3. The first excited level gives $\delta \approx 90°$, thus it is located close to the $a_1(1260)$ resonance mass and $m_{a_1} \approx E_2$ holds.

The Breit-Wigner parametrization

$$\frac{-\sqrt{s}\,\Gamma(s)}{s - (m^{\text{res}})^2 + i\sqrt{s}\,\Gamma(s)} = \frac{1}{\cot\delta - i}\,, \quad \Gamma_{a_1}(s) \equiv g_{a_1\rho\pi}^2\,\frac{p}{s}\,, \tag{6.3}$$

gives $\Gamma_{a_1}(s)$ in terms of the phase space and the coupling $g_{a_1\rho\pi}$. We obtain

$$\frac{p}{\sqrt{s}}\,\cot\delta(s) = \frac{1}{g_{a_1\rho\pi}^2}[(m_{a1}^{\text{res}})^2 - s]\,, \tag{6.4}$$

which applies in the vicinity of the resonance. Assuming that (like it is the case for the ρ) linearity (6.4) is a good approximation down to the threshold and slightly below it, we interpolate linearly in s between the two values of $p\cot\delta/\sqrt{s}$ of table 3, as shown in figure 2. From the zero and the slope we obtain $m_{a_1}^{\text{res}}$ and $g_{a_1\rho\pi}$.

The resulting parameters of the $a_1(1260)$ resonance are compared to experiment in table 5. The value of m_{a1}^{res} at $m_\pi = 266$ MeV is slightly higher than that of the experimental resonance $a_1(1260)$. This first lattice result for $g_{a_1\rho\pi}$ is valuable since there is still considerable uncertainty on the total width Γ_{a_1} and on the $a_1 \to \rho\pi$ branching ratio. We provide the upper limit for $g_{a_1\rho\pi}^{\text{exp}}$ resulting from the total width $\Gamma_{a1}^{\text{exp}} = 250 - 600$ MeV [8][3], which agrees with our $g_{a_1\rho\pi}$ within the large experimental and theoretical uncertainties. Our lattice result for $g_{a_1\rho\pi}$ is also close to the value $g_{a_1\rho\pi}^{phen} \approx 0.9$ GeV obtained using an Unitarized Effective Field Theory approach [23] (converted to our convention).

The scattering length $a_{l=0}^{\rho\pi}$ in table 5 is obtained using the effective range fit $p\cot(\delta) = \frac{1}{a_0} + \frac{1}{2}r_0p^2$ through two energy levels. Our result at $m_\pi = 266$ MeV is close to $a_{l=0}^{\rho\pi}(m_\pi^{phys}) \approx 0.37$ fm obtained from Unitarized Effective Field Theory [42], while the corresponding experimental value is not known.

7 Analysis of the b_1 channel

The robust features of the b_1 spectrum in figure 1 and in table 4 go along with the expectations: the level $\omega(0)\pi(0)$ near the $m_\omega + m_\pi$ threshold, the next level close to $b_1(1235)$ with $\delta \simeq 90^\circ$ and the third level in vicinity of $b_1(1960)$.

However the exact position of the central value for the ground state E_1 in figure 1 with respect to the threshold $m_\omega + m_\pi$ shows a slight disagreement with the expectation. It is expected to be slightly below threshold due to an attractive interaction in the resonant channel. Since $\Gamma_{b_1} < \Gamma_{a_1}$ one expects a smaller size of the energy shift $\Delta E_1 = E_1 - m_V - m_\pi$ in the b_1 channel than in the a_1 channel, rendering a lattice extraction challenging. We estimate the expected energy shift $a\Delta E_1 \simeq -0.01$ based on $g_{b_1\omega\pi}^{\text{exp}}$, Breit-Wigner dependence (6.4), the Lüscher relation (6.2) and the value of $m_{b_1}^{\text{res}}$ (7.1) determined below; note that this shift is smaller than the uncertainty of the ground state energy level in the b_1 channel and comparable to the uncertainty in am_ω. A correlated analysis reveals that our ground state E_1 is compatible with $m_\omega + m_\pi$ within the large uncertainties, although the central value leads to $E_1 \gtrsim m_\omega + m_\pi$. We stress that this discrepancy with expectations is not statistically significant.

If upon improving the statistics the ground state level still stays above threshold, this would be hard to understand. The three-pion state, for example, could hardly explain such behavior since the lowest state $\pi(0)\pi(1)\pi(-1)$ with $J = 1$ has energy $\simeq 1.6$ GeV, which is significantly above the threshold on our lattice.

In the $b_1(1235) \to \omega\pi$ channel the d-wave to s-wave amplitude ratio observed in experiment is 0.277 ± 0.027 [8], and the d-wave contribution, which we neglect in Eq. (6.2), might play an important role as it for example does in the deuteron.

[3] More precisely we assume $\Gamma_{a_1} = 425(175)$ MeV.

Due to the discussed uncertainty of the ground state energy level we determine the resonance $b_1(1235)$ mass using the Breit-Wigner relation (6.4),

$$m_{b_1}^{\text{res}} = \left[E_2^2 + (g_{b_1\omega\pi}^{\text{exp}})^2 \left(\frac{p \cot \delta}{\sqrt{s}} \right)^2 \right]^{1/2} = 1.414(36)(^{+0}_{-83}) \text{ GeV} , \tag{7.1}$$

based on E_2 and $(p \cot \delta/\sqrt{s})_2$ for the second level in table 4, while we assume the experimental value of the coupling $g_{b_1\omega\pi}^{\text{exp}} = 0.787(25)$ GeV. It is derived from $\Gamma_{b_1}^{\text{exp}}$ assuming $Br[b_1 \to \omega\pi] \simeq 1$, which has not been measured but is expected to be valid to a good approximation. The resulting resonance mass at our m_π is somewhat higher than the experimental one.

8 Conclusions and outlook

We presented the first lattice simulation of light axial resonances a_1 and b_1 taking into account their dominant strong decays modes $\rho\pi$ and $\omega\pi$. The interpolating fields $\overline{q}q$ as well as $V\pi$ ($V = \rho, \omega$) were used for this purpose. We find an energy level near the $V(0)\pi(0)$ threshold and excited levels close to the resonance positions of $a_1(1260)$ and $b_1(1235)$. The s-wave phase shifts for $V\pi$ scattering were extracted using the Lüscher relation and they are fitted using the Breit-Wigner formula. The resonance parameters are compared to experiment in table 5.

The resonance masses $m_{a_1}^{\text{res}}$ and $m_{b_1}^{\text{res}}$ at our $m_\pi \simeq 266$ MeV are somewhat higher than the experimental values. The $a_1 \to \rho\pi$ coupling $g_{a_1\rho\pi}$, which parametrizes the corresponding decay width, agrees with experiment within sizable error bars. The analogous $b_1 \to \omega\pi$ coupling was not extracted since the central value for the ground state in the b_1 channel is found slightly above $m_\omega + m_\pi$, while one expects it to be slightly below threshold in an attractive channel. The ground state is still consistent with $m_\omega + m_\pi$ and an attractive interaction within the sizable uncertainty. Future lattice studies with improved statistical accuracy could clarify this issue by resolving smaller energy shifts which should lead to a determination of $g_{b_1\omega\pi}$ from Lattice QCD.

Our analysis assumes stable scattering particles ρ and ω, which is a reasonable approximation for our simulation with zero momentum, $L \simeq 2$ fm and $m_\pi \simeq 266$ MeV. However, the effects of vector meson decays might have to be taken into account in future simulations with physical pion masses, multiple box sizes and possibly non-zero total momenta. Proper treatment of this problem appears considerably more challenging. An analytic framework for the scattering of unstable particles in finite volume has been recently proposed in [30] while the related problem of three particles where two of them can resonate was considered in [31–34]. These approaches can serve as a guideline for future lattice simulations.

A Wick contractions and the correlation matrix

A.1 The $\rho\pi$ s-wave correlation matrix

The correlation matrix is built from four operators $\mathcal{O}_{1-3}^{\overline{q}q}$ and $\mathcal{O}^{\rho\pi}$ listed in Eq. (5.1). The Wick contractions are listed in figure 3, where solid lines denote u/d quarks, while dashed

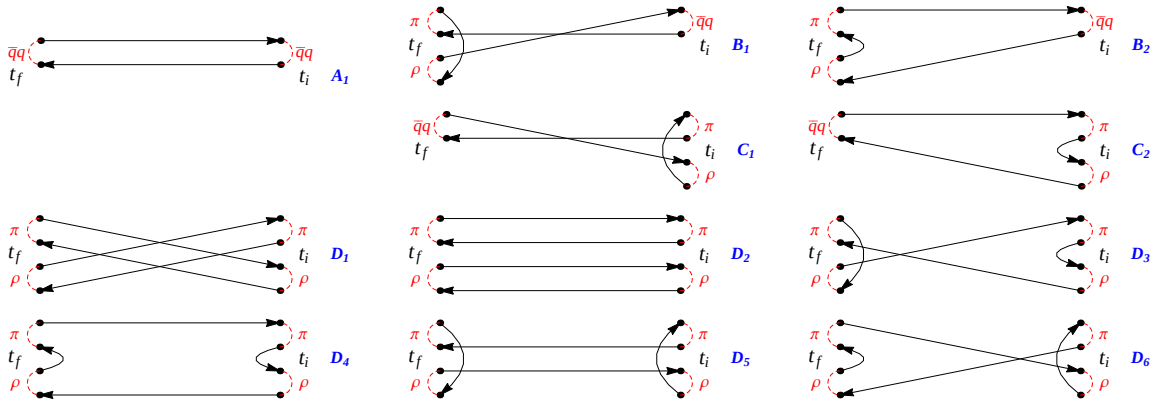
$\bar{q}q$ t_f $\bar{q}q$ t_i A_1
π t_f ρ $\bar{q}q$ t_i B_1
π t_f ρ $\bar{q}q$ t_i B_2
$\bar{q}q$ t_f π t_i ρ C_1
$\bar{q}q$ t_f π t_i ρ C_2
π t_f ρ π t_i ρ D_1
π t_f ρ π t_i ρ D_2
π t_f ρ π t_i ρ D_3
π t_f ρ π t_i ρ D_4
π t_f ρ π t_i ρ D_5
π t_f ρ π t_i ρ D_6

Figure 3. Wick contractions in the a_1 channel with $\mathcal{O}^{\bar{q}q}$ and $\mathcal{O}^{\rho\pi}$ interpolators.

lines denote the momentum projections and Dirac structures at source and sink. The correlation matrix $C(t_f, t_i)$ for the a_1 channel is built from the following linear combinations of the Wick contractions

$$\begin{aligned}
\langle O^{\bar{q}q}(t_f)\mathcal{O}^{\bar{q}q\dagger}(t_i)\rangle &= -A_1 \ , \\
\langle O^{\rho\pi}(t_f)\mathcal{O}^{\bar{q}q\dagger}(t_i)\rangle &= B_1 - B_2 \ , \\
\langle O^{\bar{q}q}(t_f)\mathcal{O}^{\rho\pi\dagger}(t_i)\rangle &= C_1 - C_2 \ , \\
\langle O^{\rho\pi}(t_f)\mathcal{O}^{\rho\pi\dagger}(t_i)\rangle &= -D_1 + D_2 + D_3 - D_4 - D_5 + D_6 \ ,
\end{aligned} \tag{A.1}$$

where $A_l,\ B_l,\ C_l,\ D_l$ refer to labels in figure 3.

A.2 The $\omega\pi$ s-wave correlation matrix

This correlation matrix is built from five operators $\mathcal{O}^{\bar{q}q}_{1-4}$ and $\mathcal{O}^{\omega\pi}$ listed in (5.2). In this case there is a larger number of Wick contractions, all drawn in figure 4. The correlation matrix is built from these Wick contractions as follows

$$\begin{aligned}
\langle O^{\bar{q}q}(t_f)\mathcal{O}^{\bar{q}q\dagger}(t_i)\rangle &= -A_1 \ , \\
\langle O^{\omega\pi}(t_f)\mathcal{O}^{\bar{q}q\dagger}(t_i)\rangle &= \sqrt{2}B_1 - \frac{1}{\sqrt{2}}B_2 - \frac{1}{\sqrt{2}}B_3 \ , \\
\langle O^{\bar{q}q}(t_f)\mathcal{O}^{\omega\pi\dagger}(t_i)\rangle &= \sqrt{2}C_1 - \frac{1}{\sqrt{2}}C_2 - \frac{1}{\sqrt{2}}C_3 \ , \\
\langle O^{\omega\pi}(t_f)\mathcal{O}^{\omega\pi\dagger}(t_i)\rangle &= +D_1 - \frac{1}{2}D_2 - 2D_3 + D_4 - \frac{1}{2}D_5 \\
&\quad + D_6 + D_7 - \frac{1}{2}D_8 - \frac{1}{2}D_9 - \frac{1}{2}D_{10} - \frac{1}{2}D_{11} + D_{12} \ .
\end{aligned} \tag{A.2}$$

Acknowledgments

We thank Anna Hasenfratz for providing the gauge configurations used for this work. We are grateful for valuable discussions with M. Döring, E. Oset, J. Pelaez, L. Roca and A.

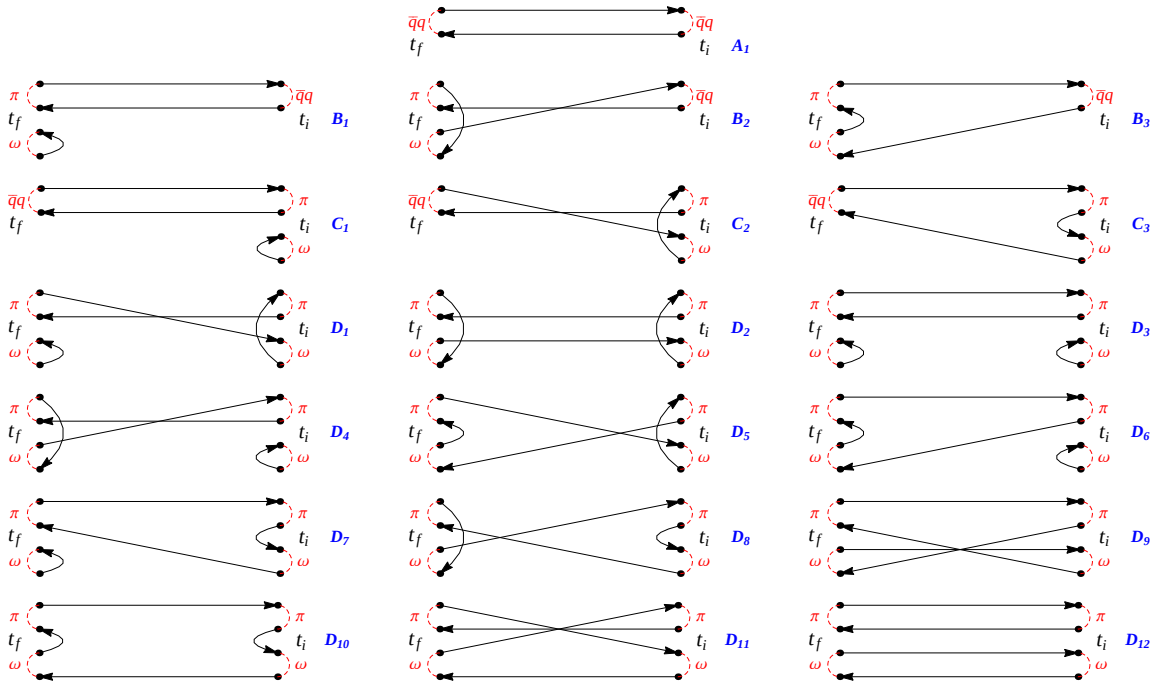

Figure 4. Wick contractions in the b_1 channel with $\mathcal{O}^{\bar{q}q}$ and $\mathcal{O}^{\omega\pi}$ interpolators.

Rusetsky. This work is supported by the Slovenian Research Agency. Fermilab is operated by Fermi Research Alliance, LLC under Contract No. De-AC02-07CH11359 with the United States Department of Energy. We thank INT in Seattle for hospitality.

References

[1] **CP-PACS** Collaboration, S. Aoki, M. Fukugita, K.-I. Ishikawa, N. Ishizuka, K. Kanaya, Y. Kuramashi, Y. Namekawa, M. Okawa, K. Sasaki, A. Ukawa, and T. Yoshi, *Lattice QCD Calculation of the ρ Meson Decay Width*, *Phys. Rev. D* **76** (2007) 094506, [arXiv:0708.3705].

[2] X. Feng, K. Jansen, and D. B. Renner, *Resonance Parameters of the rho-Meson from Lattice QCD*, *Phys. Rev. D* **83** (2011) 094505, [arXiv:1011.5288].

[3] C. B. Lang, D. Mohler, S. Prelovsek, and M. Vidmar, *Coupled channel analysis of the rho meson decay in lattice QCD*, *Phys. Rev. D* **84** (2011) 054503, [arXiv:1105.5636].

[4] **PACS-CS** Collaboration, S. Aoki, K. I. Ishikawa, N. Ishizuka, K. Kanaya, Y. Kuramashi, Y. Namekawa, M. Okawa, Y. Taniguchi, A. Ukawa, N. Ukita, T. Yamazaki, and T. Yoshié, *ρ Meson Decay in 2+1 Flavor Lattice QCD*, *Phys. Rev. D* **84** (2011) 094505, [arXiv:1106.5365].

[5] C. Pelissier and A. Alexandru, *Resonance parameters of the rho-meson from asymmetrical lattices*, *Phys. Rev. D* **87** (2013) 014503, [arXiv:1211.0092].

[6] J. J. Dudek, R. G. Edwards, and C. E. Thomas, *Energy dependence of the ρ resonance in $\pi\pi$ elastic scattering from lattice QCD*, *Phys. Rev.* **87** (2013) 034505, [arXiv:1212.0830].

[7] S. Prelovsek, L. Leskovec, C. B. Lang, and D. Mohler, *K pi scattering and the K* decay width from lattice QCD*, *Phys. Rev. D* **88** (2013) 054508, [arXiv:1307.0736].

[8] **Particle Data Group** Collaboration, J. Beringer et al., *Review of particle physics*, *Phys. Rev. D* **86** (Jul, 2012) 010001.

[9] J. Basdevant and E. L. Berger, *Unitary Coupled-Channel Analysis of Diffractive Production of the a1 Resonance*, *Phys. Rev. D* **16** (1977) 657.

[10] N. A. Tornqvist, *The A1 Mass From $\tau \to A1$ Neutrino Decay*, *Z. Phys. C* **36** (1987) 695.

[11] **COMPASS** Collaboration, M. G. Alekseev et al., *Observation of a $J^{\rm PC} = 1^{-+}$ exotic resonance in diffractive dissociation of* 190 GeV/c π^- *into* $\pi^-\pi^-\pi^+$, *Phys. Rev. Lett.* **104** (Jun, 2010) 241803.

[12] M. Lüscher, *Volume dependence of the energy spectrum in massive quantum field theories. I. Stable particle states*, *Commun. Math. Phys.* **104** (1986) 177.

[13] M. Lüscher, *Volume dependence of the energy spectrum in massive quantum field theories. II. Scattering states*, *Commun. Math. Phys.* **105** (1986) 153.

[14] M. Lüscher, *Two-Particle States on a Torus and Their Relation to the ScatteringMatrix*, *Nucl. Phys. B* **354** (1991) 531.

[15] M. Lüscher, *Signatures of unstable particles in finite volume*, *Nucl. Phys. B* **364** (1991) 237.

[16] **UKQCD** Collaboration, C. McNeile and C. Michael, *Decay width of light quark hybrid meson from the lattice*, *Phys. Rev.* **D73** (2006) 074506, [hep-lat/0603007].

[17] **UKQCD** Collaboration, C. McNeile, C. Michael, and P. Pennanen, *Hybrid meson decay from the lattice*, *Phys. Rev. D* **65** (2002) 094505, [hep-lat/0201006].

[18] S. Prelovsek, C. B. Lang, D. Mohler, and M. Vidmar, *Decay of rho and a1 mesons on the lattice using distillation*, *PoS* **LAT2011** (2011) 137, [arXiv:1111.0409].

[19] S. Weinberg, *Precise relations between the spectra of vector and axial vector mesons*, *Phys. Rev. Lett.* **18** (1967) 507–509.

[20] M. Lutz and E. Kolomeitsev, *On meson resonances and chiral symmetry*, *Nucl.Phys.* **A730** (2004) 392–416, [nucl-th/0307039].

[21] M. Wagner and S. Leupold, *Tau decay and the structure of the a(1)*, *Phys. Lett. B* **670** (2008) 22–26, [arXiv:0708.2223].

[22] M. Wagner and S. Leupold, *Information on the structure of the a(1) from tau decay*, *Phys. Rev. D* **78** (2008) 053001, [arXiv:0801.0814].

[23] L. Roca, E. Oset, and J. Singh, *Low lying axial-vector mesons as dynamically generated resonances*, *Phys. Rev.* **D72** (2005) 014002, [hep-ph/0503273].

[24] L. Geng, E. Oset, J. Pelaez, and L. Roca, *Nature of the axial-vector mesons from their N(c) behavior within the chiral unitary approach*, *Eur.Phys.J.* **A39** (2009) 81–87, [arXiv:0811.1941].

[25] L. Y. Glozman, *Restoration of chiral and $U(1)_A$ symmetries in excited hadrons*, *Phys. Rep.* **444** (2007) 1, [hep-ph/0701081].

[26] L. Y. Glozman, C. B. Lang, and M. Schröck, *Symmetries of hadrons after unbreaking the chiral symmetry*, *Phys. Rev. D* **86** (2012) 014507, [arXiv:1205.4887].

[27] A. Hasenfratz, R. Hoffmann, and S. Schaefer, *Low energy chiral constants from epsilon-regime simulations with improved Wilson fermions*, *Phys. Rev. D* **78** (2008) 054511, [arXiv:0806.4586].

[28] A. Hasenfratz, R. Hoffmann, and S. Schaefer, *Reweighting towards the chiral limit*, *Phys. Rev. D* **78** (2008) 014515, [arXiv:0805.2369].

[29] **Hadron Spectrum** Collaboration, M. Peardon, J. Bulava, J. Foley, C. Morningstar, J. Dudek, R. G. Edwards, B. Joo, H.-W. Lin, D. G. Richards, and K. J. Juge, *A novel quark-field creation operator construction for hadronic physics in lattice QCD*, *Phys. Rev. D* **80** (2009) 054506, [arXiv:0905.2160].

[30] L. Roca and E. Oset, *Scattering of unstable particles in a finite volume: the case of $\pi\rho$ scattering and the $a_1(1260)$ resonance*, *Phys. Rev. D* **85** (2012) 054507, [arXiv:1201.0438].

[31] M. T. Hansen and S. R. Sharpe, *Relativistic, model-independent, three-particle quantization condition*, [arXiv:1311.4848].

[32] K. Polejaeva and A. Rusetsky, *Three particles in a finite volume*, *Eur.Phys.J.* **A48** (Mar., 2012) 67, [arXiv:1203.1241].

[33] R. A. Briceno and Z. Davoudi, *Three-particle scattering amplitudes from a finite volume formalism*, *Phys.Rev.* **D87** (2013) 094507, [arXiv:1212.3398].

[34] R. A. Briceno, *On the Determination of Elastic and Inelastic Nuclear Observables from Lattice QCD*, arXiv:1311.6032.

[35] M. Döring, J. Haidenbauer, U.-G. Meißner, and A. Rusetsky, *Dynamical coupled-channel approaches on a momentum lattice*, *Eur. Phys. J.* **A47** (2011) 163, [arXiv:1108.0676].

[36] M. T. Hansen and S. R. Sharpe, *Multiple-channel generalization of Lellouch-Lüscher formula*, *Phys. Rev. D* **86** (2012) 016007, [arXiv:1204.0826].

[37] E. Garzon, R. Molina, A. Hosaka, and E. Oset, *Strategies for an accurate determination of the X(3872) energy from QCD lattice simulations*, arXiv:1310.0972.

[38] C. Michael, *Adjoint Sources in Lattice Gauge Theory*, *Nucl. Phys. B* **259** (1985) 58.

[39] M. Lüscher and U. Wolff, *How to calculate the Elastic Scattering Matrix in 2-Dimensional QuantumField Theories by Numerical Simulation*, *Nucl. Phys. B* **339** (1990) 222.

[40] B. Blossier, M. DellaMorte, G. von Hippel, T. Mendes, and R. Sommer, *On the generalized eigenvalue method for energies and matrix elements in lattice field theory*, *JHEP* **0904** (2009) 094, [arXiv:0902.1265].

[41] **COMPASS** Collaboration, S. Paul et al., *Precision spectroscopy with COMPASS and the observation of a new iso-vector resonance*, [arXiv:1312.3678].

[42] L. Roca and E. Oset, private communication.